

# Phase Diagram of Half Doped Manganites.

Luis Brey

*Instituto de Ciencia de Materiales de Madrid (CSIC), Cantoblanco, 28049 Madrid, Spain.*

An analysis of the properties of half-doped manganites is presented. We build up the phase diagram of the system combining a realistic calculation of the electronic properties and a mean field treatment of the temperature effects. The electronic structure of the manganites are described with a double exchange model with cooperative Jahn-Teller phonons and antiferromagnetic coupling between the  $Mn$  core spins. At zero temperature a variety of electronic phases as ferromagnetic (FM) charge ordered (CO) orbital ordered (OO), CE-CO-OO and FM metallic, are obtained. By raising the temperature the CE-CO-OO phase becomes paramagnetic (PM), but depending on the electron-phonon coupling and the exchange coupling the transition can be direct or through intermediate states: a FM disorder metallic, a PM-CO-OO or a FM-CO-OO. We also discuss the nature of the high temperature PM phase in the regime of finite electron phonon coupling. In this regime half of the oxygen octahedra surrounding the  $Mn$  ions are distorted. In the weak coupling regime the octahedra are slightly deformed and only trap a small amount of electronic charge, rendering the system metallic consequentially. However in the strong coupling regime the octahedra are strongly distorted, the charge is fully localized in polarons and the system is insulator.

PACS numbers: 75.47.Gk, 75.10.-b, 75.30.Kz, 75.50.Ee.

## I. INTRODUCTION

Oxides of composition  $(R_{1-x}A_x)MnO_3$  where R denotes rare earth ions and A is a divalent alkaline ion, are called generically manganites. In these compounds  $x$  coincides with the concentration of holes moving in the  $e_g$  orbital band of the Mn ions that ideally form a cubic structure. The electronic and magnetic properties of manganites are determined by the competition between at least four independent energy scales; the antiferromagnetic interaction between the Mn spins, the electron phonon coupling, the electronic repulsion and the kinetic energy of the carriers. In manganites the energy magnitude of these effects is the same and very different states can have very similar energies. Consequently slightly varying parameters as carrier concentration, strain, disorder, temperature etc, different phases can be experimentally observed.

In this work we calculate the phase diagram of manganites at half doping,  $x=1/2$ . We study the different phases of the system as function of temperature ( $T$ ), electron-phonon coupling ( $\lambda$ ) and antiferromagnetic superexchange coupling between the classical  $Mn$   $t_{2g}$  core spins ( $J_{AF}$ ). In particular we are interested in analyzing the different phase transitions that undergoes the paramagnetic phase when the temperature is lowered[1, 2].

Previous temperature phase diagrams have been obtained for the one orbital double exchange model[3, 4, 5]. Although this model clarifies some physics of the manganites at low hole doping, the one orbital model is insufficient for describing the complexity of half doped manganites. On the other hand Monte Carlo simulation of a two orbital double exchange model are very expensive computationally and only very small systems can

be studied[6]. In this paper the phase diagram is obtained combining the electronic properties obtained from a realistic microscopic two-dimensional Hamiltonian and a mean field treatment of the temperature fluctuations. With this method it is possible to analyze system with up to  $26 \times 26$  Mn ions, and the results are rather free of finite size effects. It has been shown extensively[7] that, due to the directionality of the electronic active  $e_g$  Mn orbitals, the phases appearing in two-dimensional calculations are qualitatively similar to those appearing in three-dimensional models, and the zero temperature phase diagrams obtained in two and three dimensions are topologically equivalent.

In Figures 1,2 and 3 we show the main results of this work. Fig.1 shows the phase diagram  $T - \lambda$  of the half-doped two-dimensional, two orbital double exchange model with cooperative Jahn-Teller phonons for  $J_{AF}=0.06t$ . In Fig.2 and 3 we plot the  $T - J_{AF}$  phase diagrams for  $\lambda=1.6t$  and  $\lambda=2t$  respectively. Here  $t$  is the hopping between first neighbors  $d_{x^2-y^2}$  orbitals in the  $x-y$  plane, and in the rest of the paper it is taken as the unit of energy.

The magnetic phases appearing in the diagram are: ferromagnetic (FM), antiferromagnetic (AF), paramagnetic (PM) and CE (ferromagnetic zigzag chains that are coupled antiferromagnetically[8]). In some phases the electric charge is chessboard-like ordered (CO phases). The charge modulation is due to the cooperative Jahn-Teller coupling. The electronic charge trapped in a  $Mn$  ion depends on the distortion of the oxygen octahedron surrounding the ion, that at the same time depends on  $\lambda$ . The octahedra distortions of first neighbors  $Mn$  ions are coupled and due to the elastic energy a distorted octahedron is encircled by undistorted octahedra. The order

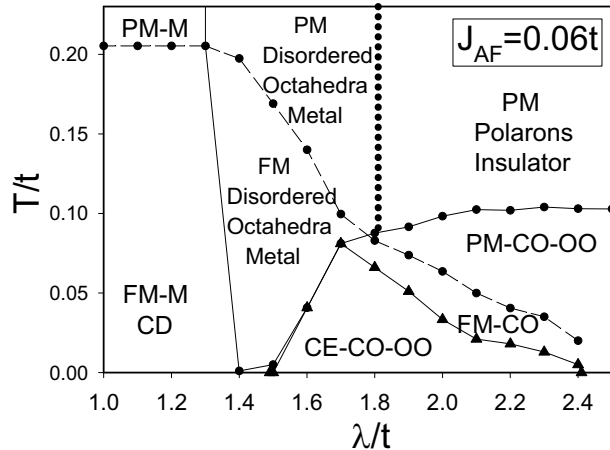


FIG. 1: Phase diagram,  $T$ - $\lambda$ , for the two dimensional DE two orbital model with cooperative Jahn-Teller phonons. The AF coupling is  $J_{AF}=0.06t$ . The abbreviations explaining the phases are defined in the text. First order transitions are indicated by continuous lines and second order transitions by dashed lines. The big dot line indicates a metal-insulator transition. The PM-M is also CD, and the FM-CO is also OO. Note that for  $1.4t < \lambda < 1.5t$  and low  $T$  there is a small region, almost imperceptible in the figure, where the system is FM-CO-OO.

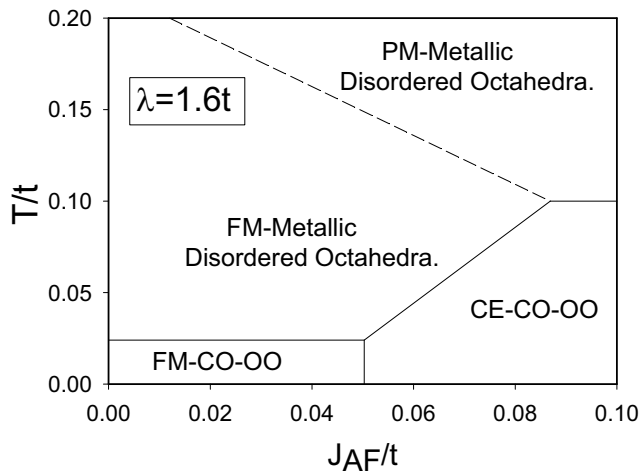


FIG. 2: Phase diagram,  $T$ - $J_{AF}$ , for the two dimensional DE two orbital model with cooperative Jahn-Teller phonons. The Jahn-Teller coupling is  $\lambda=1.6t$ . The abbreviations explaining the phases are defined in the text. First order transition are indicated by continuous lines and second order transitions by dashed lines.

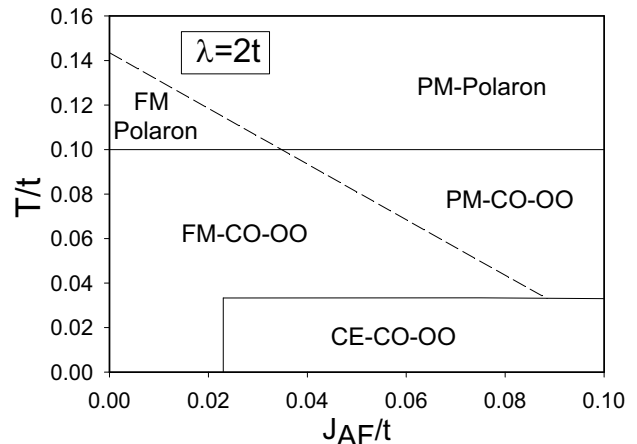


FIG. 3: Same than Fig. 2 but with  $\lambda=2t$ .

in the octahedra distortions produces the electron charge modulation. For large values of the coupling,  $\lambda \geq 2.3t$ , the charge modulation is maximum and the CO phase is an ordered distribution of  $Mn^{3+}$  and  $Mn^{4+}$ . However for weaker values of  $\lambda$  the modulation is much smaller. The cooperative nature of the Jahn-Teller coupling implies that the CO is concomitant to the existence of orbital ordering (OO). Charge disordered (CD) names metallic phases (M) where the electric charge moves freely between the  $Mn$  ions and is equally distributed between them. For strong Jahn-Teller coupling,  $\lambda \geq 1.9t$ , by raising  $T$  the CO phase melts into an insulator polaron-like state where the carriers are practically fully localized in  $Mn$  ions surrounded by a strong distorted oxygen octahedron. For weak values of  $\lambda$  the CO phase melts into a state formed of weak deformed oxygen octahedra, that trap only a small amount of the electronic charge. This phase is metallic and can be considered as a *crossover* between the normal Fermi liquid phase and the polaron-like state[9, 10]. In the phase diagrams, Figures 1,2 and 3, the solid and the dashed lines represent first and second order phase transitions respectively. In Fig 1 the large dot line separating the disordered octahedra metallic phase from the polaron-like state, is an estimation of the value of  $\lambda$  where the system undergoes a metal-insulator transition. Some of the high temperature phases appearing in Figures 1,2 and 3 have been not reported in Monte Carlo simulations. We believe that due to size effects the disordered octahedra phases could be difficult to identified in small systems.

Due to computational limitations we have only considered spatially uniform phases in Figures 1,2 and 3. Therefore we can not rule out the existence of more sophisticated spatially commensurate/incommensurate modulated phases[11, 12, 13, 14, 15, 16]. In the calculation we have not considered coupling between different

order parameters. This could affect or phase diagram near crossing between different lines of phase transitions. Also near the crossing points the thermal fluctuations that are neglected in the mean field approximation could be important.

Some characteristics of the phase diagrams explain several experimental results on manganites and deserves to be discussed explicitly:

i) There is a region on the parameter space, small  $J_{AF}$  large  $\lambda$ , where the zero temperature ground state is FM and presents charge and orbital ordering, FM-CO-OO. This phase results from the cooperative JT phonon and does not require a strong  $J_{AF}$  coupling to exist [6, 17]. A phase with the same symmetry has been observed recently by Loudon *et al.* [18].

ii) In agreement with several experimental results [19, 20, 21, 22, 23, 24] and theoretical works [7, 25, 26, 27, 28] there is a wide region of the phase diagram (intermediate values of  $\lambda$  and  $J_{AF}$ ), where the low temperature ground state is the insulator CE-CO-OO phase.

iii) At high temperature the system is always paramagnetic, but depending on the value of the electron phonon coupling the system behaves as a metal (low  $\lambda$ ) a disorder metal (moderate values of  $\lambda$ ) or an insulator (strong coupling). These regimes have been observed experimentally. In the case of  $\text{La}_{0.5}\text{Sr}_{0.5}\text{MnO}_3$  [29] the high temperature paramagnetic phase is metallic, whereas in perovskites with strong electron-phonon coupling, as  $\text{La}_{0.5}\text{Ca}_{0.5}\text{MnO}_3$  [1] the paramagnetic phase is an insulator.

iv) By raising the temperature the CE-CO-OO insulating phase becomes a PM phase, but depending on the values of  $\lambda$  and  $J_{AF}$ , in the heating process the transition is through a FM disorder metallic phase or through a PM-CO-OO phase. These phase transition paths describe appropriately the experimental phenomenology. Upon cooling,  $\text{La}_{0.5}\text{Ca}_{0.5}\text{MnO}_3$  first becomes FM-CO and then CE [1, 30], however in the case of  $\text{Pr}_{0.5}\text{Ca}_{0.5}\text{MnO}_3$ , the intermediate phase is a PM-CO phase [2, 15].

This article is organized as follows. In Sec. II we describe the model and the approximations used to find the energies and properties of the different phases. In Sec. III, we describe the phases studied and outline the method for obtaining the critical temperatures and the transitions between the phases. In Sec. IV we summarize the results.

## II. MODEL.

We assume that the manganites crystallize in an ideal perovskites structure where the Mn ions form a cubic lattice. The crystal field splits the Mn  $d$  levels into an occupied strongly localized  $t_{2g}$  triplet and a doublet of  $e_g$  symmetry. The Coulomb interaction between electrons prevents double occupancy and aligns the spins of the  $d$  orbitals. At  $x \neq 1$  there is a finite density of electrons in the system that hop between the empty  $e_g$  Mn states.

The Hund's coupling between the spins of the carriers and each core spin is much larger than any other energy in the system, and each electron spin is forced to align locally with the core spin texture. Then the carriers can be treated as spinless particles and the hopping amplitude between two Mn ions is modulated by the spin reduction factor,

$$f_{12} = \cos \frac{\vartheta_1}{2} \cos \frac{\vartheta_2}{2} + e^{i(\phi_1 - \phi_2)} \sin \frac{\vartheta_1}{2} \sin \frac{\vartheta_2}{2} \quad (1)$$

where  $\{\vartheta_i, \phi_i\}$  are the Euler angles of the, assumed classical, Mn core spins  $\{\mathbf{S}_i\}$ . This is the so called DE model [31, 32, 33].

For obtaining the states of the system we study a two dimensional DE model coupled to Jahn-Teller (JT) phonons. We also include the AF coupling between the Mn core spins  $J_{AF}$ .

$$\begin{aligned} H = & - \sum_{i,j,a,a'} f_{i,j} t_{a,a'}^u C_{i,a}^+ C_{j,a'} \\ & + J_{AF} \sum_{\langle i,j \rangle} \mathbf{S}_i \mathbf{S}_j + \frac{1}{2} \sum_i (\beta Q_{1i}^2 + Q_{2i}^2 + Q_{3i}^2) \\ & + \lambda \sum_i (Q_{1i} \rho_i + Q_{2i} \tau_{xi} + Q_{3i} \tau_{zi}) , \end{aligned} \quad (2)$$

here  $C_{i,a}^+$  creates an electron in the Mn ions located at site  $i$  in the  $e_g$  orbital  $a$  ( $a=1,2$  with  $1=|x^2 - y^2\rangle$  and  $2=|3z^2 - r^2\rangle$ ). The hopping amplitude is finite for next neighbors Mn and depends both on the type of orbital involved and on the direction  $u$  between sites  $i$  and  $j$  ( $t_{1,1}^{x(y)} = \pm \sqrt{3} t_{1,2}^{x(y)} = \pm \sqrt{3} t_{2,1}^{x(y)} = 3 t_{2,2}^{x(y)} = t$ ) [7].  $t$  is taken as the energy unit. The fourth term couples the  $e_g$  electrons with the three active  $\text{MnO}_6$  octahedra distortions: the breathing mode  $Q_{1i}$ , and the JT modes  $Q_{2i}$  and  $Q_{3i}$  that have symmetry  $x^2 - y^2$  and  $3z^2 - r^2$  respectively.  $Q_{1i}$  couples with the charge at site  $i$ ,  $\rho_i = \sum_a C_{i,a}^+ C_{i,a}$  whereas  $Q_{2i}$  and  $Q_{3i}$  couple with the  $x$  and  $z$  orbital pseudospin,  $\tau_{xi} = C_{i1}^+ C_{i2} + C_{i2}^+ C_{i1}$  and  $\tau_{zi} = C_{i1}^+ C_{i1} - C_{i2}^+ C_{i2}$ , respectively. The third term is the elastic energy of the octahedra distortions, being  $\beta \geq 2$  the spring constant ratio for breathing and JT-modes [6]. In the perovskite structures the oxygens are shared by neighbouring  $\text{MnO}_6$  octahedra and the  $Q$ 's distortions are not independent, cooperative effects being very important [5]. In order to consider these collective effects we consider the position of the oxygen atoms as the independent variables of the JT distortions.

For a given value of the parameters  $\lambda$  and  $J_{AF}$ , and a texture of core spins  $\{\mathbf{S}_i\}$ , we solve self-consistently the mean field version of Hamiltonian (2) and obtain the energy, the local charges  $\{\rho_i\}$ , the orbital pseudospin order  $\{\tau_{xi}, \tau_{zi}\}$  and the oxygen octahedra distortions  $Q_{\alpha,i}$ . These quantities are better described by their Fourier transforms, that are represented by the same symbol with a hat:  $\hat{\rho}(\mathbf{G})$ ,  $\hat{Q}_1(\mathbf{G})$ , ... We have checked that with our model and the appropriated parameters we recover some well known states as the FM and the CE-CO [6, 7, 26].

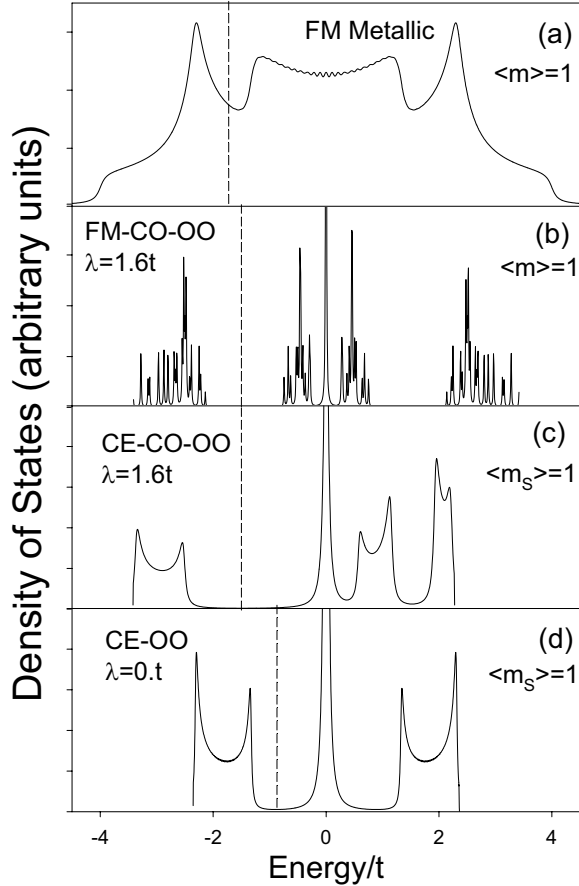


FIG. 4: Density of states for different ordered phases (see text). The dashed lines indicate the position of the Fermi energy. The density of states of the FM-CO-OO phase is discrete as it is obtained by solving numerically a system with  $24 \times 24$   $Mn$  ions.

Therefore we are in a position for studying other phases that can appear at half doping.

### III. ELECTRIC AND MAGNETIC PHASES AND CRITICAL TEMPERATURES.

#### A. Ferromagnetic Metallic (FM-M) phase.

In this phase the  $Mn$  spins point, on average, in a particular direction, and there is a finite relative magnetization  $\langle m \rangle$ . In the spirit of the virtual crystal approximation, we consider a unique value for the spin reduction factor  $f_{ij}$  that corresponds to its expectation value,

$$f_{ij} \simeq \left\langle \sqrt{\frac{1 + \cos \theta_{ij}}{2}} \right\rangle \simeq \sqrt{\frac{1 + \langle \cos \theta_{ij} \rangle}{2}} = \sqrt{\frac{1 + \langle m \rangle^2}{2}}, \quad (3)$$

where  $\langle \rangle$  means thermal average,  $\theta_{ij}$  represents the angle formed by the spins located at sites  $i$  and  $j$ . In Eq.(3) we have approached the expectation value of the square root by the square root of the average value[34]. This phase occurs for small values of  $J_{AF}$  and  $\lambda$  for which the octahedra are not distorted and the system is metallic. In Fig.4(a) we plot the density of states (DOS) of the FM metallic phase for  $\langle m \rangle = 1$ . For other values of the magnetization the bandwidth is  $8t\sqrt{\frac{1 + \langle m \rangle^2}{2}}$ . The internal energy is the sum of an electronic energy and the AF superexchange energy,

$$E^{FM-M} = \varepsilon_{FM} \sqrt{\frac{1 + \langle m \rangle^2}{2}} + 2J_{AF} \langle m \rangle^2. \quad (4)$$

Here  $\varepsilon_{FM}$  is the electronic energy per  $Mn$  ion in the full polarized ( $\langle m \rangle = 1$ ) ferromagnetic metallic phase. The paramagnetic phase corresponds to a random orientation of the  $Mn$  spins,  $\langle m \rangle = 0$ . Both the ferromagnetic and paramagnetic metallic phases do not present charge ordering, however in order to minimize the kinetic energy, the  $x^2-y^2$  orbital is more occupied than the  $3z^2-r^2$  orbital[6] and these phases show orbital ordering. The occurrence of orbital order in a metallic phase only happen in two dimensions and therefore, here, we do not consider it as a relevant effect.

In order to describe thermal effects we have to compute the free energy. In the manganites, the typical critical temperatures are lower than 300K and the thermal energy is much smaller than the electronic energies,  $t \sim 0.2eV$ , and neglect thermal effects on the carriers Fermi distribution is a good approximation. Therefore we only need to consider the entropy of the classical  $Mn$  spins. We use the molecular field approximation, neglecting all correlations between different spins and assuming for each of them a statistical distribution corresponding to an effective magnetic field  $h$ [33]. The free energy of a system of classical spins in presence of  $h$  is

$$\mathcal{F} = -\frac{1}{\beta} \log \left( 2 \frac{\sinh(\beta h)}{\beta h} \right), \quad (5)$$

and the magnetization of this system is

$$\langle m \rangle = -\frac{\partial \mathcal{F}}{\partial h} = \frac{1}{\tanh(\beta h)} - \frac{1}{\beta h}. \quad (6)$$

This equation gives the relation between the effective magnetic field and the magnetization. The entropy of the spin system is given by

$$-TS = \mathcal{F} - \langle m \rangle h = \frac{1}{\beta} \left( -\log \left( 2 \frac{\sinh(\beta h)}{\beta h} \right) - m\beta h \right), \quad (7)$$

that can be written as a function of  $\langle m \rangle$  solving self-consistently Eq.5 and Eq.6. In the limit of small magnetization the entropy takes the form,

$$S(\langle m \rangle) = \frac{\log 2}{2} - \frac{3}{2} \langle m \rangle^2 - \frac{9}{20} \langle m \rangle^4 + \dots \quad (8)$$

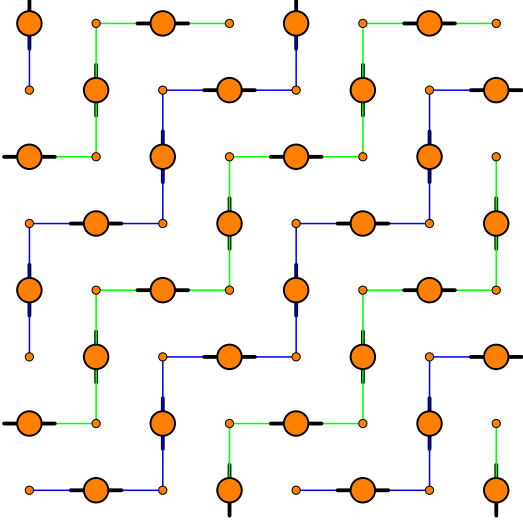


FIG. 5: (Color online) Schematic view of CO-OO phases. The horizontal and vertical lines on the lattice sites represent the positive and negative oxygen octahedra distortions. The size of the dots is proportional to the charge located on the  $Mn$  ions. In the case of  $\lambda=1.6t$  the octahedra distortion is  $Q_2=\pm 1.25t$  and the ions have charge 0.71 and 0.29. In the FM phase all ions have the same spin orientation, whereas the CE phase consists of FM zigzag chains which are coupled AF.

Using this expression for the  $Mn$  spins entropy the total free energy of the system near the PM to FM transition takes the form,

$$\begin{aligned}
 F(\langle m \rangle) &= E^{FM-M} - TS(\langle m \rangle) \\
 &\approx F(0) + \langle m \rangle^2 \left( \frac{3}{2} T + \frac{\varepsilon_{FM}}{2\sqrt{2}} + 2J_{AF} \right) \\
 &\quad + \langle m \rangle^4 \left( \frac{9}{20} T - \frac{\varepsilon_{FM}}{8\sqrt{2}} \right) + \dots \quad (9)
 \end{aligned}$$

and the Curie temperature is

$$T_C = -\frac{\varepsilon_{FM}}{3\sqrt{2}} - \frac{4}{3} J_{AF} . \quad (10)$$

The constant multiplying the  $\langle m \rangle^4$  term is positive and therefore the transition is a second order phase transition.

### B. Ferromagnetic, Charge Ordered, Orbital Ordered phase (FM-CO-OO).

For small values of  $J_{AF}$  and strong enough electron phonon coupling,  $\lambda \gtrsim 1.4t$ , the ground state present

charge and orbital order and a finite relative magnetization,  $\langle m \rangle \neq 0$ . This is a surprising state as the charge order (CO) is normally associated with AF order. In manganites the CO is created by the electron phonon coupling and for realistic values of  $\lambda$ , the charge disproportionation between the two different types of  $Mn$  ions is small. Then the system can reduce its energy by ordering ferromagnetically the  $Mn$  core spins and minimizing the kinetic energy.

The charge ordering is characterized by a single Fourier component,  $(\pi, \pi)$ , of the charge density,  $\hat{\rho}(\pi, \pi) \neq 0$ . The orbital ordering is described by a uniform  $z$ -orbital pseudospin,  $\tau_{z,i}$  and two finite Fourier components of the  $x$ -component of the pseudospin,  $\hat{\tau}_x(\pi/2, \pi/2) = \hat{\tau}_x(-\pi/2, -\pi/2) \neq 0$ . Due to the electron phonon coupling, the amplitude of the charge modulation is related with the distortion of the oxygen octahedra,  $\hat{Q}_2(\pi/2, \pi/2) = \hat{Q}_2(-\pi/2, -\pi/2) \neq 0$ , that depends on the value of  $\lambda$ . The sites where the electron charge is larger than the average,  $x=1/2$ , the  $Q_2$  mode has a finite value, whereas the octahedra surrounding  $Mn$  ions with less charge than the average are undistorted. The sign and amplitude of the distortion are modulated in order to minimize the elastic energy of the cooperative Jahn-Teller distortion. The CO-OO phase can be described as a distribution of deformed octahedra. The position of the distorted octahedra determines the electron charge ordering, and the orientation of the octahedra distortions fix the orbital ordering in the system. CO and OO are a consequence of the spatial modulation of the octahedra deformations. In Fig. 5 we plot the arrangement of the octahedra distortion and the electronic charge distribution for a unit cell with  $8 \times 8$   $Mn$  ions for  $\lambda=1.6t$ . As the  $Mn$  ions have two orbitals per site, the  $(\pi/2, \pi/2)$  modulation of the octahedra distortion opens a gap at the Fermi energy for  $x=1/2$  and therefore the system is an insulator. The magnitude of the gap increases with the value of  $\lambda$ . In Fig.4(b) we plot a typical density of this phase for  $\lambda=1.6t$ .

A decrease of the relative magnetization  $\langle m \rangle$  produces a reduction in the spin reduction factor  $f_{i,j}$  and in the kinetic energy, making the relative electron-phonon interaction stronger. The internal energy per  $Mn$  ion of this phase can be written as

$$E^{FM-CO} = \varepsilon_{FM-CO}(\lambda, \langle m \rangle) + 2J_{AF} \langle m \rangle^2 . \quad (11)$$

where the electronic energy depends in a complicated way on  $\lambda$  and  $\langle m \rangle$  and has to be obtained numerically by solving Eq.(2).

The Curie temperature of the FM-CO-OO phase can be calculated similarly to the FM-M case, and we obtain

$$T_C = -\frac{2}{3} \frac{\partial E^{FM-CO}}{\partial \langle m \rangle^2} \Big|_{\langle m \rangle=0} . \quad (12)$$

In the case of the FM-CO-OO phase the derivative has to be obtained numerically. From higher derivatives of

the internal energy with respect to the magnetization we obtain that the transition is second order.

### C. CE, Charge Order, Orbital Order phase (CE-CO-OO).

Magnetically the CE phase consists of ferromagnetic zigzag chains coupled ferromagnetically. The horizontal and vertical steps of the chain contain three Mn ions. For finite values of the electron phonon coupling the charge, orbitals and octahedra distortions are ordered similarly to in the FM-CO-OO phase. In the case of  $\lambda=0$ , the CE phase does not present charge order, however due to the dependence of the electron hopping in the spatial direction, the system spontaneously creates an orbital order similar to that occurring in the FM-CO-OO phase,  $\hat{r}_z(0,0) \neq 0$  and  $\hat{r}_x(\frac{\pi}{2}, \frac{\pi}{2}) = \hat{r}_x(-\frac{\pi}{2}, -\frac{\pi}{2}) \neq 0$ . Independently of the existence of charge modulation the  $(\frac{\pi}{2}, \frac{\pi}{2})$  orbital order opens a gap at the Fermi energy and the half doped system is an insulator. In the  $\lambda=0$  case the gap is just due to the orbital order and the system is classified as a band insulator[35]. In Fig. 4(c)and(d), we plot the density of states in the CE phase for  $\lambda=1.6t$  and  $\lambda=0$  respectively. There is a gap at the Fermi energy that for  $\lambda=0$  is of the order of the hopping parameter,  $t$ , and that increases with the electron phonon coupling.

For each value of  $\lambda$  there is a minimal value of  $J_{AF}$  for the occurrence the CE-OO-CO phase. At zero temperature and for  $\lambda=0$  the minimal AF coupling is  $J_{AF} \simeq 0.18t$ , whereas for  $\lambda=1.6t$  and  $\lambda=2t$  the minimal AF coupling are  $0.05t$  and  $0.023t$  respectively, Figures 2 and 3.

The magnetization of the CE phase is described by the relative amount of saturation in each zigzag chain  $\langle m_S \rangle$ . In the virtual crystal approximation the fluctuations are neglected and the hopping is modulated by the spin reduction factor that is different along the zigzag FM chain,  $f^{FM}$  than between the AF coupled chains,  $f^{AF}$ [33],

$$\begin{aligned} f^{FM} &= \sqrt{\frac{1 + \langle m_S \rangle^2}{2}} \\ f^{AF} &= \sqrt{\frac{1 - \langle m_S \rangle^2}{2}} . \end{aligned} \quad (13)$$

The internal energy of this phase depends on  $\lambda$ , and  $\langle m_S \rangle$  and can be written as,

$$E^{CE-CO} = \varepsilon_{CE-CO}(\lambda, \langle m_S \rangle) . \quad (14)$$

As each  $Mn$  spin core is surrounded by two  $Mn$  spins coupled FM and other two coupled AF, the superexchange energy is zero.

In order to compute the Neel temperature of the CE phases, we introduce an effective field for each spin sublattice. Taking into account that both, the magnetization and the effective magnetic field, have different sign in each sublattice, we obtain the same expression for the entropy than in the FM phase, but just changing  $\langle m \rangle$

by  $\langle m_S \rangle$ [33]. With this the free energy takes the form,

$$\begin{aligned} F(\langle m_S \rangle, \lambda) &= E^{CE-CO} - TS(\langle m_S \rangle) \\ &\simeq F(0) + \langle m_S \rangle^2 \left( \frac{3}{2}T + a \right) \\ &+ \langle m_S \rangle^4 \left( \frac{9}{20}T + b \right) + \dots \end{aligned} \quad (15)$$

with

$$E^{CE-OO} \approx cte + a \langle m_S \rangle^2 + b \langle m_S \rangle^4 + \dots \quad (16)$$

Due to the symmetry of the CE phase the coefficient  $a$  is zero, and the Neel temperature gets the form

$$T_N^{CE} = -\frac{20}{9}b. \quad (17)$$

Numerically, we obtain  $b < 0$  and therefore there is a finite temperature first order phase transition. As it is shown in Fig. 1-3, only for large values of  $\lambda$  and  $J_{AF}$  the CE-OO-OO phase transforms directly into the PM-CO-OO. At smaller values of  $\lambda$  and  $J_{AF}$  the transition to the PM phase is through a FM-CO-OO (Fig 1) or through a FM metallic disordered octahedra phase (Fig. 2).

### D. Antiferromagnetic CO-OO phase

For large values of  $J_{AF}$ , the kinetic energy is zero and the electron charge is fully localized forming a chessboard-like pattern of  $Mn^{3+}$  and  $Mn^{4+}$ . For finite values of  $\lambda$  the octahedra surrounding the  $Mn^{3+}$  ions are distorted cooperatively and the system presents OO and has the same symmetry than the others CO-OO phases. The minimal value of  $J_{AF}$  for the occurrence of this phase depends on  $\lambda$ , but in general is rather large, and this phase is unlikely to occur in half doped manganites, and it in this work is not considered.

### E. Disordered octahedra phases: Polaron phase and metallic crossover phase.

At high temperature the CO phases melt. The nature of the disorder high temperature phase depends on the strength of the electron phonon interaction. The melting of a charge density wave is a complicated problem, and only recently it has been possible to apply an unique treatment for studying the weak and the strong coupling regimes[9, 10]. Part of the difficulty in studying the melting of a charge density wave is to define the order parameter that vanishes in the disordered phase. In the manganites this problem can be avoided by considering the distribution of the distorted oxygen octahedra instead of the modulation of the charge density. In the CO-OO phases there are two order parameters,  $\xi$ , describing the order-disorder transition in the the spatial distribution of the distorted oxygen octahedra and  $\eta$ , parameterizing

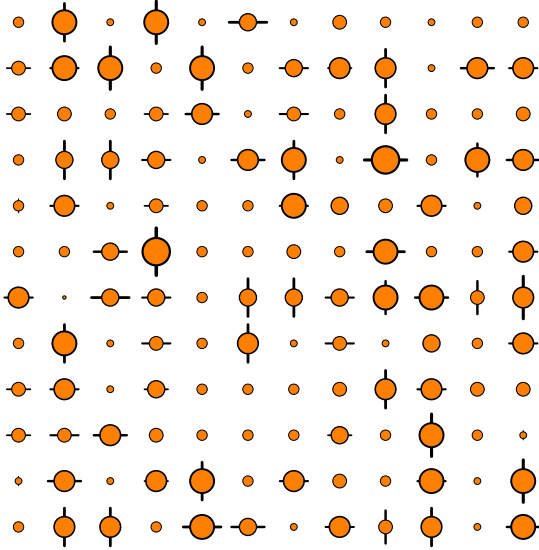


FIG. 6: (Color online) Schematic view of the disordered octahedra phase for moderate values of  $\lambda$ . The horizontal and vertical lines on the lattice sites represent the positive and negative oxygen octahedra distortions. The size of the dots is proportional to the charge located on the  $Mn$  ions. For  $\lambda=1.6t$  the octahedra distortion is  $Q_2=\pm 0.95t$ , and the charge located on the  $Mn$  ions is in the range 0.25-0.75.

their orientational order. The octahedra distorted phase can exist on a FM or PM  $Mn$  spins background. However, we have not found any region in the parameter space where the stable phase contains a disorder distribution of octahedra on a magnetic CE background.

The free energy of the CO-OO phases has the form,

$$F(\xi, \eta) = F(0, 0) - T \left( S_M(\xi) + \frac{1}{2} S_M(\eta) \right) + E^{CO-OO}(\xi, \eta), \quad (18)$$

being  $S_M$  the entropy of mixing[36],

$$S_M(x) = \ln 2 - \frac{1}{2}(1+x) \ln(1+x) - \frac{1}{2}(1-x) \ln(1-x), \quad (19)$$

and  $E^{CO-OO}(\xi, \eta)$  the electronic internal energy measured with respect to the full disordered case. Near  $\xi=0$  and  $\eta=0$ , the internal energy can be expanded as

$$E^{CO-OO}(\xi, \eta) = \sum_{n,m} a_{n,m} \xi^n \eta^m \quad (20)$$

we have evaluated numerically the lower coefficients in this expansion and we have found a strong coupling between the two order parameters that indicates the first order nature of the order disorder transition. Assuming a transition between the fully disordered phase and the fully ordered phase the melting critical temperature of

the CO-OO phases is

$$T_M = -\frac{2}{3 \ln 2} (E^{CO-OO}(1, 1) - E^{CO-OO}(0, 0)) \quad (21)$$

In order to compute the energy of the disordered octahedra phase we locate randomly the distorted octahedra ( $\xi=0$ ). The sign of the distortion is also random ( $\eta=0$ ). We assume that all the octahedra have the same elongation amplitude,  $Q_2$ , and we find its value by minimizing the energy. For a given value of the electron phonon coupling the value of the deformation  $Q_2$  is smaller in the disorder phase than in the CO-OO phases. We have checked in several cases that the energy is minimized when the number of distorted octahedra and the number of electrons is the same.

By changing the value of  $\lambda$ , the octahedra disordered phase has different behaviors. There is a critical value of  $\lambda$  where the distortion  $Q_2$  become finite. As can be observed in Fig.1, this value,  $\lambda \sim 1.3t$ , is slightly smaller than the critical  $\lambda$  for the zero temperature FM to CO-OO transition ( $\lambda \sim 1.4t$  for  $J_{AF}=0.06t$ ). This decrease occurs because the spin reduction factor is smaller, and the relative electron phonon coupling larger, in the PM phase than in the FM phase. For values of  $\lambda$  larger than the critical value, but not too strong, the mode  $Q_2$  is small and the distorted octahedra only trap a small amount of electronic charge, see Fig.(6). Interestingly the disorder in the position and orientation of the Mn octahedra creates states in the energy gap region of the insulating ordered phase that favor transport of charge making the system to behave as a metal[37, 38]. In Fig.7(a) we plot the density of states for a realization of the disordered octahedra phase for  $\lambda=1.6t$  in a system containing  $24 \times 24$   $Mn$  ions. The amplitude of the distortion that minimizes the energy is  $Q_2=0.95$ . There is not gap in the DOS, and there is a finite number of disorder induced states at the Fermi energy. It is interesting to compare this DOS with that of the ordered phases calculated with the same  $\lambda$ , Fig. 4(c)-(d). The energy gap of the ordered phase disappears when disorder in the positions and orientation of the octahedra is introduced. The states at the Fermi energy transport electric charge and the metallic behavior of this phase is reflected in the low frequency spectral weight of the optical conductivity  $\sigma(\omega)$ , Fig.8(a), that shows a clear Drude-like character.

By increasing  $\lambda$  the octahedra distortion increases, the electronic charge becomes strongly localized, and the system is a disordered mixing of  $Mn^{3+}$  and  $Mn^{4+}$ . We name this state polaronic phase. In Fig.9 a typical octahedra distribution and electron charge in the polaronic regime,  $\lambda=2t$ , is plotted. Note that the electron charge is practically localized on  $Mn$  ions surrounded by a distorted oxygen octahedron. In this strong coupling regime the DOS shows a fully occupied polaron band and a strong suppression of states at the Fermi energy as can be observed in Fig. 7(b). This is an indication of the insulator behaviour of this phase, being more evident in the optical conductivity Fig.8(b), that shows a strong reduction

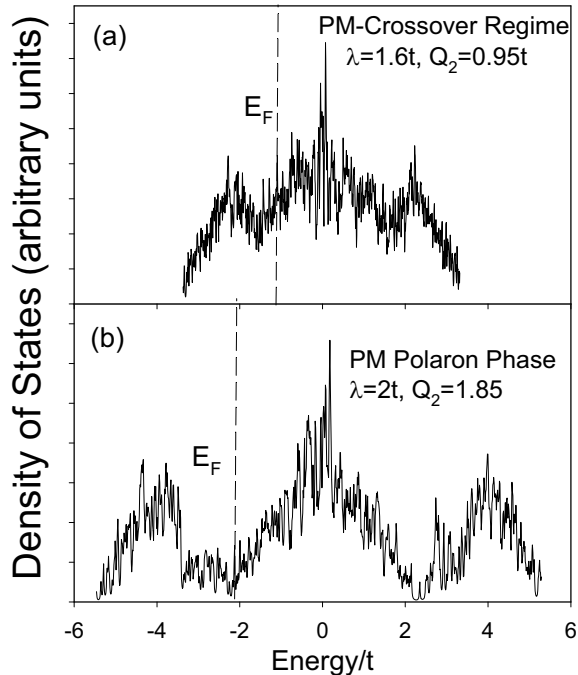


FIG. 7: Density of states of the disordered octahedra phase in the case of (a)  $\lambda=1.6t$  and (b)  $\lambda=2t$ . The dashed lines indicate the position of the Fermi energy. The density of states is obtained by solving numerically a system with  $24 \times 24$   $Mn$  ions per unit cell.

of the low energy weight and the development of a gap structure.

Although is very difficult to calculate numerically the critical value of  $\lambda$  for the metal insulating transition in the disordered octahedra phase, by comparing qualitatively the DOS and the optical conductivity we estimate,  $\lambda \sim 1.5t$ , as the critical value of the electron phonon coupling (Fig.1).

#### IV. SUMMARY

We have calculated the phase diagram of manganites at half doping. By combining a realistic microscopic electronic model and a mean field treatment of thermal effects, we have obtained the free energy of the different possible states. With these ingredients we build up phase diagrams as function of temperature and electron phonon and as function of temperature and antiferromagnetic coupling. By changing the value of the electron phonon or the antiferromagnetic coupling we simulate different manganites with different controlled bandwidth. The calculated phase diagrams show a big variety of exotic phases some of them, as the CE-CO-OO and the FM-CO-OO, have been observed experimentally.

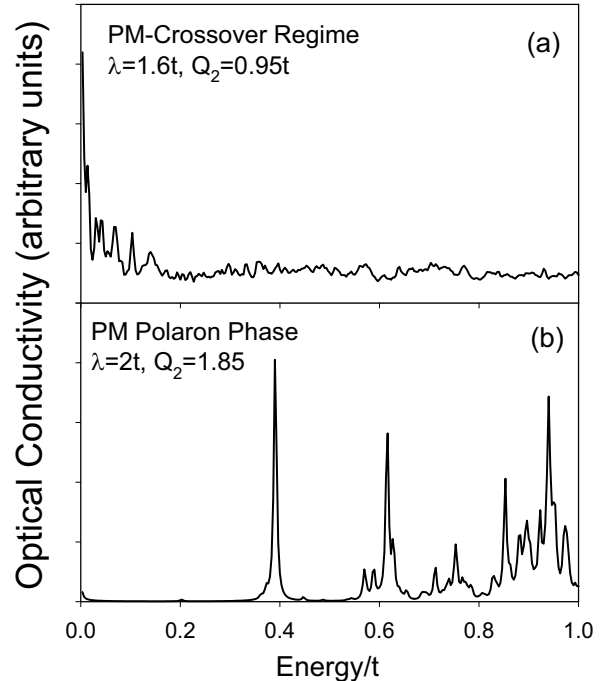


FIG. 8: Optical conductivity of the disordered octahedra phase in the case of (a)  $\lambda=1.6t$  and (b)  $\lambda=2t$ . The optical conductivity is obtained by solving numerically a system with  $24 \times 24$   $Mn$  ions per unit cell.

We have obtained that the transition from the high temperature paramagnetic phase to the low temperature CE phase, depends on the parameters  $\lambda$  and  $J_{AF}$ . For large values of  $\lambda$  the transition can be through a FM-CO-OO phase (small  $J_{AF}$ ) or trough a PM-CO-OO phase (large  $J_{AF}$ ). However for small values of  $\lambda$  the transition can be direct (large  $J_{AF}$ ) or trough a disorder FM phase (small  $J_{AF}$ ).

We have also discussed the nature of the high temperature PM phase in the regime of finite  $\lambda$ . We have obtained that in the weak coupling regime the oxygen octahedra surrounding the  $Mn$  ions are slightly distorted and only trap a small amount of electronic charge, being the system metallic. However in the strong coupling regime half of the octahedra are strongly distorted and the charge is localized in the  $Mn$ 's ions encircled by a distorted octahedron, forming a polaron and making the system insulator.

#### V. ACKNOWLEDGMENTS

The author thanks M.J.Calderón, P.B.Littlewood, N.D.Mathur and P.López-Sancho for helpful discussions. This author thanks Cambridge University for hospital-



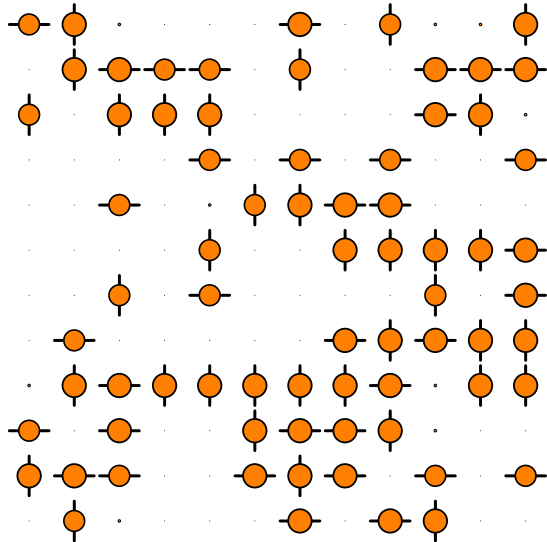


FIG. 9: (Color online) Schematic view of the disordered octahedra phase for large values of  $\lambda$ . The horizontal and vertical lines on the lattice sites represent the positive and negative oxygen octahedra distortions. The size of the dots is proportional to the charge located on the  $Mn$  ions. For  $\lambda=2t$  the octahedra distortion is  $Q_2=\pm 1.85 t$ , and the electrons are practically fully localized in the  $Mn$  ions surrounded by distorted octahedra.

ity during the realization of this work. Financial support is acknowledged from Grants No MAT2002-04429-C03-01 (MCyT, Spain), Fundación Ramón Areces and Secretaria de Estado de Universidades. The work at Cambridge was partially supported by the UK EPSRC.

- 
- [1] P.Schiffer, A.P.Ramirez, W.Bao, and S.-W.Cheong, Phys. Phys. Lett. **75**, 3336 (1995).
- [2] N. C. S.Mori, T.Karsufuji and S.-W.Cheong, Phys. Phys. B **59**, 13573 (1999).
- [3] M. J. Calderón and L. Brey, Phys. Rev. B **58**, 3286 (1998).
- [4] J. Alonso, J.A.Capitán, L. A. Fernández, F. Guinea, and V. Martín-Mayor, Phys. Rev. B **64**, 054408 (2001).
- [5] J. A. Vergés, V. Martín-Mayor, and L. Brey, Phys. Rev. Lett **88**, 136401 (2002).
- [6] H. Aliaga, D. Magnoux, A. Moreo, D. Poilblanc, S. Yunoki, and E. Dagotto, Phys. Rev. B **68**, 104405 (2003).
- [7] E. Dagotto, *Nanoscale Phase Separation and Colossal Magnetoresistance* (Springer-Verlag, Berlin, 2002).
- [8] E.O.Wollan and W. Koehler, Phys. Rev. **100**, 545 (1955).
- [9] S.Ciuchi and F. Pasquale, Phys. Rev. B **59**, 5431 (1999).
- [10] S.Blawid and A.Millis, Phys. Rev. B **62**, 2424 (2000).
- [11] N.Mathur and P.Littlewood, Solid State Commun. **119**, 1509 (2001).
- [12] G. Milward, M. Calderon, and P. Littlewood, condmat/0407727.
- [13] L. Brey, Phys.Rev.Lett. **92**, 127202 (2004).
- [14] C.H.Chen and S.-W.Cheong, Phys. Phys. Lett. **76**, 4042 (1996).
- [15] R.Kajimoto, H.Yoshizawa, Y.Tomioka, and Y.Tokura, Phys. Rev. B **63**, 212407 (2001).
- [16] J.C.Loudon, S.Cox, A.J.Williams, J.P.Attfield, P.B.Littlewood, P.A.Midgley, and N.D.Mathur, condmat/0308581.
- [17] T.Hotta, A.Feiguin, and E.Dagotto, Phys. Rev. Lett. **86**, 4922 (2001).
- [18] J.C.Loudon, N.D.Mathur, and P. Midgley, Nature **420**, 797 (2002).
- [19] J.B.Goodenough, Phys. Rev. **100**, 564 (1955).
- [20] P.G.Radaelli, D.E.Cox, M.Marezio, and S.-W.Cheong, Phys. Rev. B **55**, 3015 (1997).
- [21] Y.Tomioka and Y.Tokura, Phys. Rev. B **66**, 104416 (2002).
- [22] F.Rivadulla, E.Winkler, J.-S.Zhou, and J.B.Goodenough, Phys. Rev. B **66**, 174432 (2002).
- [23] A.Daoud-Aladine, J.Rodriguez-Carvajal, L.Pinsard-Gaudart, M.T.Fernández-Díaz, and A.Revcolevschi, Phys. Rev. Lett. **89**, 097205 (2002).
- [24] S.Greiner, J.P.Hill, D.Gibbs, K.J.Thomas, M.v.Zimmermann, C.S.Nelson, V.Kiryukhin, Y.Tokura, Y.Tomioka, D.Casa, et al., Phys. Rev. B **69**, 134419 (2004).
- [25] I.Solovyev and K.Terakura, Phys. Rev. Lett. **83**, 2825 (1999).

- [26] J. van den Brink, G.Khaliullin, and D.Khomskii, Phys. Rev. Lett. **83**, 5118 (1999).
- [27] V.Ferrari, M.D.Towler, and P.B.Littlewood, Phys.Rev.Lett. **91**, 227202 (2003).
- [28] M. J. Calderón, A.J.Millis, and K.H.Ahn, Phys. Rev. B **69**, 100401 (2003).
- [29] A.Urushibara, Y.Moritono, T.Arima, A.Asamisu, G.Kido, and Y.Tokura, Phys. Phys. B **51**, 14103 (1995).
- [30] F.Rivadulla, M.Freita-Alvite, M.López-Quintela, L.E.Hueso, D.R.Miguerés, P.Sande, and J.Rivas, J.Appl.Phys. **91**, 785 (2002).
- [31] C.Zener, Phys. Rev. **82**, 403 (1952).
- [32] P. Anderson and H.Hasewaga, Phys. Rev. **100**, 675 (1955).
- [33] P.-G. de Gennes, Phys. Rev. **118**, 141 (1960).
- [34] D.Arovas, G.Gómez-Santos, and F.Guinea, Phys. Rev. B **59**, 13569 (1999).
- [35] T.Hotta, Y.Takada, H.Koizumi, and E.Dagotto, Phys. Rev. Lett. **84**, 2477 (2000).
- [36] P.M.Chaikin and T.C.Lubensky, *Principles of Condensed Matter Physics* (Cambridge University Press, Cambridge, UK, 1995).
- [37] N. Y.Motome and N.Nagaosa, Phys.Rev.Lett. **91**, 167204 (2003).
- [38] G. C.Sen and E.Dagotto, cond-mat/0401619.